RSC Advances

PAPER

View Article Online
View Journal | View Issue

Cite this: *RSC Adv.*, 2022, **12**, 20919

Phenoxy pendant isatins as potent α-glucosidase inhibitors: reciprocal carbonyl···carbonyl interactions, antiparallel π···π stacking driven solid state self-assembly and biological evaluation†‡

Saba Mehreen,[a] Mehwash Zia,[b] Ajmal Khan,[c] Javid Hussain,[d] Saeed Ullah,[c] Muhammad U. Anwar,[c] Ahmed Al-Harrasi*[c] and Muhammad Moazzam Naseer*[a]

Carbonyl–carbonyl (CO···CO) interactions are recently explored noncovalent interactions of significant interest owing to their role in the stability of biomacromolecules. Currently, substantial efforts are being made to understand the nature of these interactions. In this study, twelve phenoxy pendant isatins **1–12** have been evaluated for their α-glucosidase inhibitory potential in addition to the analysis of X-ray single crystals of **4** and **9**. Both compounds **4** and **9** showed intriguing and unique self-assembled structures. The CO···CO and antiparallel displaced π···π stacking interactions are mainly involved in the formation of 1D-stair like supramolecular chains of **4** whereas antiparallel π···π stacking interactions drive the formation of 1D-columnar stacks of **9**. These compounds not only highlight the potential of the isatin moiety in forming strong CO···CO and antiparallel π···π stacking interactions but also are interesting models to provide considerable insight into the nature of these interactions. The *in vitro* biological studies revealed that all twelve phenoxy pendant isatins **1–12** are highly potent inhibitors of α-glucosidase enzyme with IC_{50} values ranging from 5.32 ± 0.17 to 150.13 ± 0.62 μM, showing many fold more potent activity than the standard drug, acarbose (IC_{50} = 873.34 ± 1.67). Easy access and high α-glucosidase inhibition potential of these phenoxy pendant isatins **1–12** provide an attractive platform for finding more effective medication for controlling postprandial hyperglycemia.

Received 26th May 2022
Accepted 2nd July 2022

DOI: 10.1039/d2ra03307k

rsc.li/rsc-advances

1. Introduction

Owing to its varied reactivity and ubiquity, the carbonyl group holds a prominent position in both chemistry and biology.[1] Other than its involvement in a huge inventory of chemical transformations, it plays a principal role in the organization of both chemical and biological systems through non-covalent interactions including hydrogen bonding (C=O···H),[2–5] carbonyl–chalcogen interactions (C=O···X; X = S, Se, and Te)[6–11] and nucleophile–carbonyl interactions (Nu···C=O).[12,13] Based on the seminal work on nucleophile–carbonyl interactions by Bürgi *et al.*,[14–16] more recently chemists have recognized carbonyl–carbonyl (CO···CO) interactions.[17–20] CO···CO interactions are emerging noncovalent interactions which have been found to play an important role in stabilizing α-helices, β-sheets and the right-hand twist often observed in β-strands of proteins.[21,22] Since their recognition in natural systems, substantial efforts have been devoted to understanding the nature of these interactions and revealing their impact on diverse chemical and biological phenomena.[23,24] The dipolar nature of the carbonyl group creates the possibility for a variety of attractive interactions to be present between two carbonyl groups that include coulombic interactions (between point charges on the carbon of one moiety and the oxygen of another), dipolar interactions (between the permanent electric dipoles of the two groups) and donor–acceptor (n → π*) interactions (between electron-rich orbitals of one carbonyl and electron-deficient orbitals of another).[12] Recently, the "reciprocal" variant of the CO···CO interactions has been reported to have contributions from both n → π* and π → π* orbital interactions.[23,24]

Despite remarkable progress, the π···π interactions are still among the most debated non-covalent interactions.[25–27] These

[a]*Department of Chemistry, Quaid-i-Azam University, Islamabad, 45320, Pakistan. E-mail: moazzam@qau.edu.pk*

[b]*Department of Chemistry, Allama Iqbal Open University, Islamabad-44000, Pakistan*

[c]*Natural and Medical Sciences Research Centre, University of Nizwa, Birkat Almouz 616, Oman. E-mail: aharrasi@unizwa.edu.om*

[d]*Department of Biological Sciences & Chemistry, College of Arts and Sciences, University of Nizwa, Nizwa, Oman*

† Electronic supplementary information (ESI) available. CCDC 2175052 and 2175053. For ESI and crystallographic data in CIF or other electronic format see https://doi.org/10.1039/d2ra03307k

‡ Dedicated to Professor Klaus Jurkschat on occasion of his 70th birthday

interactions which are normally present in the aromatic systems are attractive targets for supramolecular chemists, not only because of their potential applications in different areas of materials and biological sciences but also to gain the fundamental understanding of their complicated nature.[25–27] For example, these interactions are found to play an imperative role in exceptional photoconductivity in organic crystals, designing of molecular shuttles, efficient charge transport channels and selective detection of nitroaromatics-based explosive materials.[28–31] These are also a vital supramolecular forces in structure and properties of biomolecules.[32–36]

Isatin (indoline-2,3-dione) is undoubtedly an important nucleus in medicinal chemistry.[37–39] Taking the advantage of its versatile reactivity, a huge library of isatin derivatives is now available with diverse applications.[37–39] Most of these derivatives have been obtained by utilizing either the nucleophilic nature of its NH or the high reactivity of its 3-carbonyl group. These derivatives are reported to have a variety of biological activities like antibacterial, antifungal, anticancer, antitubercular, antidiabetic, neuroprotective, anticonvulsant, anti-HIV, analgesic, anti-oxidant, anti-inflammatory, anti-glycation, anti-malarial, antianxiety and so on.[37–39] Very recently, an interesting feature of isatin nucleus (contains duality having electron rich six membered ring and electron deficient five-membered ring) makes it more special particularly in the field of materials/supramolecular chemistry and crystal engineering.[40] Owing to this feature, the isatin nucleus has strong tendency to form strong antiparallel π–π stacking interactions. However, these antiparallel π···π stacking interactions are usually not observed in its 3-carbonyl derivatives due to the nearby steric crowding and competing interactions.

Managing diabetes is one of the biggest challenges of 21st century.[41] Diabetes is an elevated blood glucose level (hyperglycemia) as a consequence of the endocrine disorder[41] leading to serious health issues that include cardiovascular disease,[42,43] nephropathy,[44] retinopathy,[45] encephalopathy,[46] thrombosis[47] and Alzheimer's disease.[48] International Diabetes Federation (IDF) declares it a global issue that results into deaths of millions of people every year due to associated complications.[49] One of the options to control this hyperglycemia in diabetic patients is to inhibit the digestion of dietary carbohydrates.[50] The enzyme α-glucosidase in small intestine is responsible for the hydrolyses of dietary carbohydrates such as starch and disaccharides to glucose that enters the bloodstream resulting hyperglycemia.[50,51] Consequently, the inhibition of α-glucosidase can reduce blood sugar levels by suppressing carbohydrate digestion.[50,51] Acarbose, voglibose, and miglitol are commercially available α-glucosidase inhibitors, but unfortunately they are reported to have adverse side effects like diarrhea, abdominal discomfort, bloating and flatulence.[52,53] Hence, novel and more effective α-glucosidase inhibitors are presently much needed.

In this context and as continuation of our research interests in biologically active isatin derivatives,[54–56] and non-covalent interactions,[57–62] herein we report the evaluation of *in vitro* α-glucosidase inhibitory activity of twelve phenoxy pendant isatins **1–12** (Fig. 1) in addition to solid-state structures of two

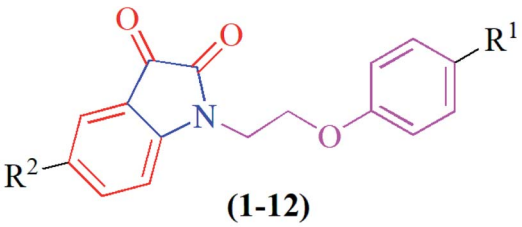

(1-12)

1. $R^1 = H, R^2 = Cl$ **7.** $R^1 = Br, R^2 = Br$
2. $R^1 = Cl, R^2 = Cl$ **8.** $R^1 = F, R^2 = Br$
3. $R^1 = Br, R^2 = Cl$ **9.** $R^1 = H, R^2 = H$
4. $R^1 = F, R^2 = Cl$ **10.** $R^1 = Cl, R^2 = H$
5. $R^1 = H, R^2 = Br$ **11.** $R^1 = Br, R^2 = H$
6. $R^1 = Cl, R^2 = Br$ **12.** $R^1 = F, R^2 = H$

Fig. 1 The structures of phenoxy pendant isatins **1–12**.

compounds **4** and **9**. The solid-state self-assemblies of **4** and **9** are primarily driven by CO···CO and antiparallel π···π stacking interactions, respectively. Most importantly, the solid-state structure of **4** represent the only example where both one-sided CO···CO and very recently discovered reciprocal CO···CO interactions are observed together. Therefore, the compound **4** may serve as the model for detailed understanding of CO···CO interactions. Similarly, the compound **9** having both antiparallel and antiparallel displaced, π···π stacking interactions offer an ideal platform to have considerable insight into the nature, strength and directionality of these debated interactions. Additionally, all the compounds **1–12** evaluated for the α-glucosidase inhibition activity are found to have potent activity much better than the standard drug, acarbose.

2. Results and discussion

2.1 Synthesis and solid state self-assembly

Phenoxy pendant isatins **1–12** (Fig. 1) were synthesized by the straightforward reaction of isatin/5-substituted isatin with 1-(2-bromoethoxy)-4-substituted benzenes.[63] The concentrated DMSO solution of phenoxy pendant isatins **4** and **9** provided good quality single crystals when placed at room temperature for a weak. The X-ray diffraction analysis of these crystals disclosed intriguing solid-state structures of these compounds. The details of X-ray crystallographic data are presented in Table 1. The phenoxy pendant isatins **4** and **9** were crystallized in the triclinic and monoclinic crystal lattice with the $P\bar{1}$ and $P2_1/c$ space groups, respectively. The molecular structures (ORTEP diagrams) of **4** and **9** containing the crystallographic numbering scheme are shown in Fig. 2. Selected geometric parameters (bond lengths (Å) & torsion angles (°) of **4** and **9** derived from the X-ray crystallographic study are described in Table 2.

In both phenoxy pendant isatins **4** and **9**, the isatin and phenoxy rings that are bridged by an ethylene moiety lie almost perpendicular to each other (Fig. 2). The conformation of

Table 1 X-ray crystallographic data of phenoxy pendant isatins **4** and **9**

Crystal data	**4**	**9**
CCDC	2175052	2175053
Chemical formula	$C_{16}H_{11}ClFNO_3$	$C_{16}H_{13}NO_3$
M_r	319.71	267.27
Crystal system, space group	Triclinic, $P\bar{1}$	Monoclinic, $P2_1/c$
Temperature (K)	296	296
a, b, c (Å)	8.324 (10), 8.326 (10), 12.233 (16)	8.912 (2), 6.7346 (16), 22.581 (6)
β (°)	92.36 (5), 106.63 (4), 116.57 (4)	96.102 (14)
V (Å^3)	712.2 (15)	1347.6 (6)
Z	2	4
Radiation type	Mo $K\alpha$	Mo $K\alpha$
μ (mm^{-1})	0.29	0.09
Crystal size (mm)	0.60 × 0.28 × 0.05	0.8 × 0.7 × 0.07
Data collection		
Diffractometer	Bruker APEX-II CCD	Bruker APEX-II CCD
Absorption correction	Multi-scan SADABS	Multi-scan SADABS
T_{min}, T_{max}	0.674, 0.745	0.538, 0.745
No. of measured, independent and observed [$I > 2\sigma(I)$] reflections	16 520, 2928, 1822	24 086, 2791, 1868
R_{int}	0.096	0.109
$(\sin\theta/\lambda)_{max}$ (Å^{-1})	0.629	0.629
Refinement		
$R[F^2 > 2\sigma(F^2)]$, $wR(F^2)$, S	0.046, 0.121, 1.03	0.082, 0.212, 1.12
No. of reflections	2928	2791
No. of parameters	199	181
H-atom treatment	H-atom parameters constrained	H-atom parameters constrained
$\Delta\rangle_{max}$, $\Delta\rangle_{min}$ (e Å^{-3})	0.23, −0.30	0.24, −0.30

central ethylene moiety in **4** and **9** is visualized as staggered gauche with the two aryl rings having a dihedral angle of N(1)–C(8)–C(7)–O(2) 60.86° and N(1)–C(1)–C(2)–O(1) −62.68°, respectively (Fig. S1†). The lone pair electrons of nitrogen of isatin in **4** and **9** may be resonating marginally towards the 3-carbonyl group as this lead to the disruption of aromaticity [N(1)–C(12) 1.422(3) Å, C(10)–C(11) 1.461(3) Å, O(4)–C(10) 1.203(3) Å in **4** and N(1)–C(12) 1.415(4) Å, C(10)–C(11) 1.453(5) Å, O(3)–C(10) 1.207(4) Å in **4**]. These electrons in fact prefer to delocalize towards the nearby 2-carbonyl groups as indicated by the relevant shorter N–C [N(1)–C(9) 1.368(3) Å in **4** and 1.359(4) Å in **9**] and slightly longer O=C [O(2)–C(9) 1.214(3) Å in **4** and O(3)–C(9) 1.212(4) Å in **9**] bond distances (Table 2). It is interesting to note here that nitrogen lone pair of isatin ring in **4** resonate less onto both carbonyls compared to the nitrogen lone pair of isatin in **9** (see bond distances in Table 2). This delocalization and the presence of two highly electronegative oxygen atoms renders the five membered ring of isatin an electron deficient ring, offering an interesting duality to the isatin that already has a fused electron rich six-membered ring.[40] Owing to this special structural feature, isatin moiety has high capability of making strong antiparallel π–π stacking interactions. However, this important feature that may lead to interesting applications of isatin derivatives in the field of materials chemistry and crystal engineering, remains largely unexplored so far.[63] Over and beyond the capability of making strong antiparallel π–π stacking interactions, the isatin moiety having two carbonyl groups have another strong possibility of making carbonyl···carbonyl interactions. As in most cases the isatin has been derivatized by using the reactivity of its 3-carbonyl, this structural feature of isatin therefore could not be noted and highlighted before.

Owing to these special structural features of isatin moiety (*vide supra*), the solid-state self-assembly of phenoxy pendant isatins **4** and **9** is dominated mainly by two types of non-covalent interactions *i.e.* CO···CO and antiparallel π···π stacking interactions (Fig. 3). Interestingly, two different types of CO···CO interactions namely, one sided interaction [C=O···C=O (T) = −70.20° and ∠C=O···C = 102.94°] where one carbonyl donates and the other carbonyl accepts and a recently discovered reciprocal interactions[24] [C=O···C=O (T) = 0° and ∠C=O···C = 85.00°] where both the carbonyl groups work as donors and acceptors, are observed in the solid-state self-assembly of **4** having 2.928 Å and 3.101 Å distances (d), respectively (Fig. 3a, S2,† Table 3). The angle θ associate with one sided CO···CO interaction is very close to the Burgi–Dunitz (BD) trajectory [∠Nu–C=O ∼ 109°] and to the relevant angles reported in the literature for this interaction.[23] However, the same angle observed for reciprocal CO···CO interactions having sheared antiparallel orientation, is smaller than that in the BD trajectory. Rahim *et al.* recently described that the donor carbonyl oxygen atoms approach the acceptor carbonyl carbon

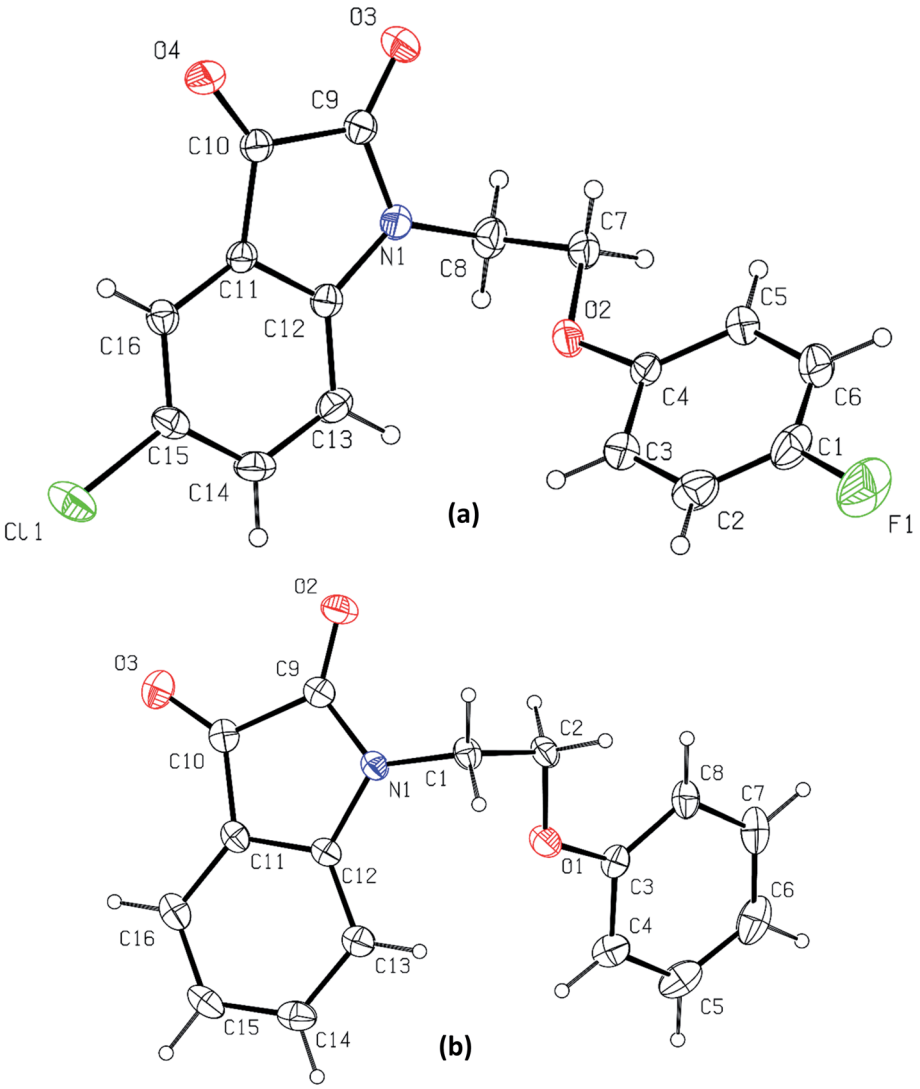

Fig. 2 The molecular structures (ORTEP diagrams) of phenoxy pendant isatins, (a) **4**; (b) **9**. Displacement ellipsoids are drawn at the 50% probability level.

Table 2 Selected geometric parameters; bond lengths (Å) and torsion angles (°) of phenoxy pendant isatins **4** and **9** derived from the X-ray crystallographic study

Compound	**4**	**9**
N(1)–C(12)	1.422(3)	1.415(4)
C(10)–C(11)	1.461(3)	1.453(5)
O(4)–C(10)/O(3)–C(10)	1.203(3)	1.207(4)
N(1)–C(9)	1.368(3)	1.359(4)
O(3)–C(9)/O(2)–C(9)	1.214(3)	1.212(4)
N(1)-C(8)-C(7)-O(2)/N(1)-C(1)-C(2)-O(1)	60.86	−62.68

atoms considerably away from the BD trajectory (∠O···C=O is ~85°) in systems having reciprocal interactions.[24] The distances observed in these CO···CO interactions are also much less than the sum of the van der Waals radii of C and O (3.22 Å) (Table 3).[64] The two isatin moieties having CO···CO interactions in **4** interact with each other by means of antiparallel displaced π··· π stacking interactions [d = 3.810 Å between the centres of six and five membered rings of two adjacent isatins (Fig. 3b)] supported by a self-complimentary CH···O [C(3)–H(3)···O(4) 2.604 Å] interactions, providing 1D-supramolecular stair-like chains (Fig. 4a). In contrast, two types of π···π stacking interactions have been observed in the solid state self-assembly of **9** (Fig. 3c and d). Rather than CO···CO interactions observed in **4**, two isatin moieties interact with each other by means of strong antiparallel π···π stacking in **9** with a distance of 3.520 Å between the centres of six and five membered rings of two adjacent isatin moieties (Fig. 3c). These stacked phenoxy pendent isatins in **9** then joins to their neighbouring stacks with the help of antiparallel displaced π···π stacking interactions [d = 3.702 Å between the centres of six and five membered rings of two adjacent isatin moieties (Fig. 3d)] assisted by a bifurcated self-complimentary CH···O and CH···π [C(16)–H(16)···O(1) 2.691 Å and C(16)–H(16)···C(3) 2.897 Å] interactions, furnishing 1D-supramolecular columnar stacks (Fig. 4b). The

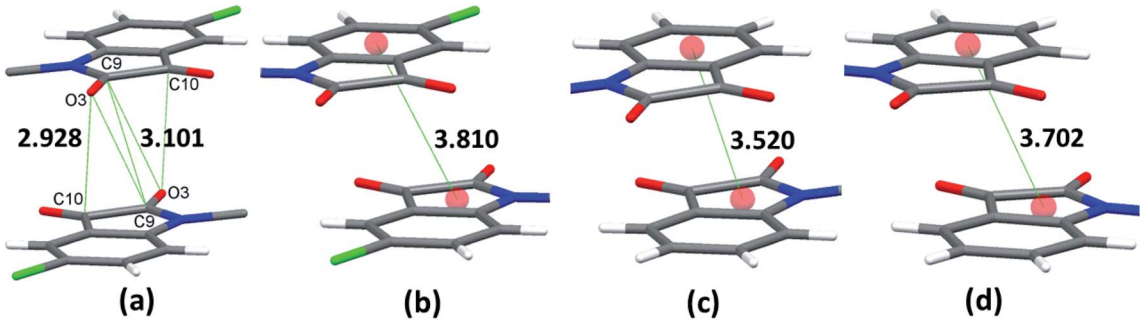

Fig. 3 Showing a) carbonyl···carbonyl interactions in **4**; b) antiparallel displaced π···π stacking interactions in **4**; c) antiparallel π···π stacking interactions in **9**; d) antiparallel displaced π···π stacking interactions in **9**.

Table 3 Geometric parameters associated with non-covalent interactions observed in the solid state self-assembly of **4** and **9**

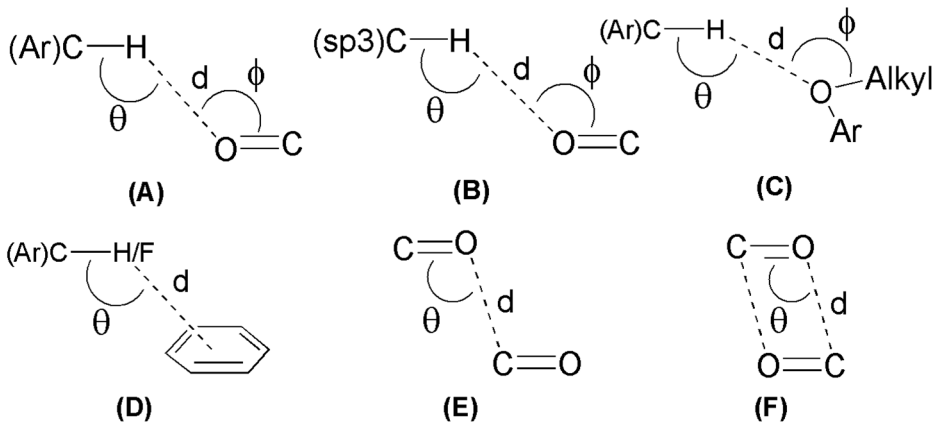

Compd	Type	Contact atoms	d (Å)	θ (°)	ϕ (°)
1	A	C(3)–H(3)···O(4)	2.604	145.44	129.42
		C(6)–H(6)···O(3)	2.610	176.01	133.48
		C(14)–H(14)···O(4)	2.538	151.14	116.58
	D	C(1)–F(1)···C(16)	3.030	158.14	—
	E	CO···CO	2.928	102.94	—
	F	CO···CO	3.101	85.00	—
2	A	C(15)–H(15)···O(2)	2.583	156.90	132.47
	B	C(1)–H(1B)···O(2)	2.640	152.77	121.42
		C(2)-H(2A)···O(2)	2.577	156.15	113.64
	C	C(16)–H(16)···O(1)	2.691	145.19	116.95
	D	C(16)–H(16)···C(3)	2.897	170.08	—
		C(5)–H(5)···C(4)	2.806	157.54	—

supramolecular 1D-stair like chains of **4** by means of CH···O [C(6)–H(6)···O(3) 2.610 Å, C(14)–H(14)···O(4) 2.538 Å] and F···π [C(1)–F(1)···C(16) 3.030 Å] interactions finally expand themselves to provide an overall 3D-network structure of **4** (Fig. 5a). Similarly, the 1D-columnar stacks of **9** attaches themselves to the neighboring columnar stacks by means of CH···O [C(15)–H(15)···O(2) 2.583 Å, C(1)-H(1B)···O(2) 2.640 Å and C(2)-H(2A)···O(2) 2.577 Å] and CH···π [C(5)–H(5)···C(4) 2.691 Å interactions to give an overall 3D-network structure of **9** (Fig. 5b).

To see the strengths of hydrogen bonds involved in crystal packing of **4** and **9**, H-bond angles θ are considered (Table 3). Generally, it is believed that the relatively linear hydrogen bonds ($150° < \theta < 180°$) are structurally more important due to dipole-monopole and dipole–dipole contribution to the electrostatic energy (maximum at $\theta = 180°$ and zero at $\theta = 90°$).[65] Careful analysis of the bond angles θ gathered in Table 3 shows that the most of involved (Ar)C–H···O and (sp^3)C–H···O interactions are relatively linear and hence significant. The angle ϕ is used to analyze the lone-pair directionality of the acceptor atom. The angle ϕ for different acceptor oxygen atoms have been observed in the range of 113.64–133.48°, indicating the sidewise approach of the hydrogen bond donors.[66] Keeping in view the

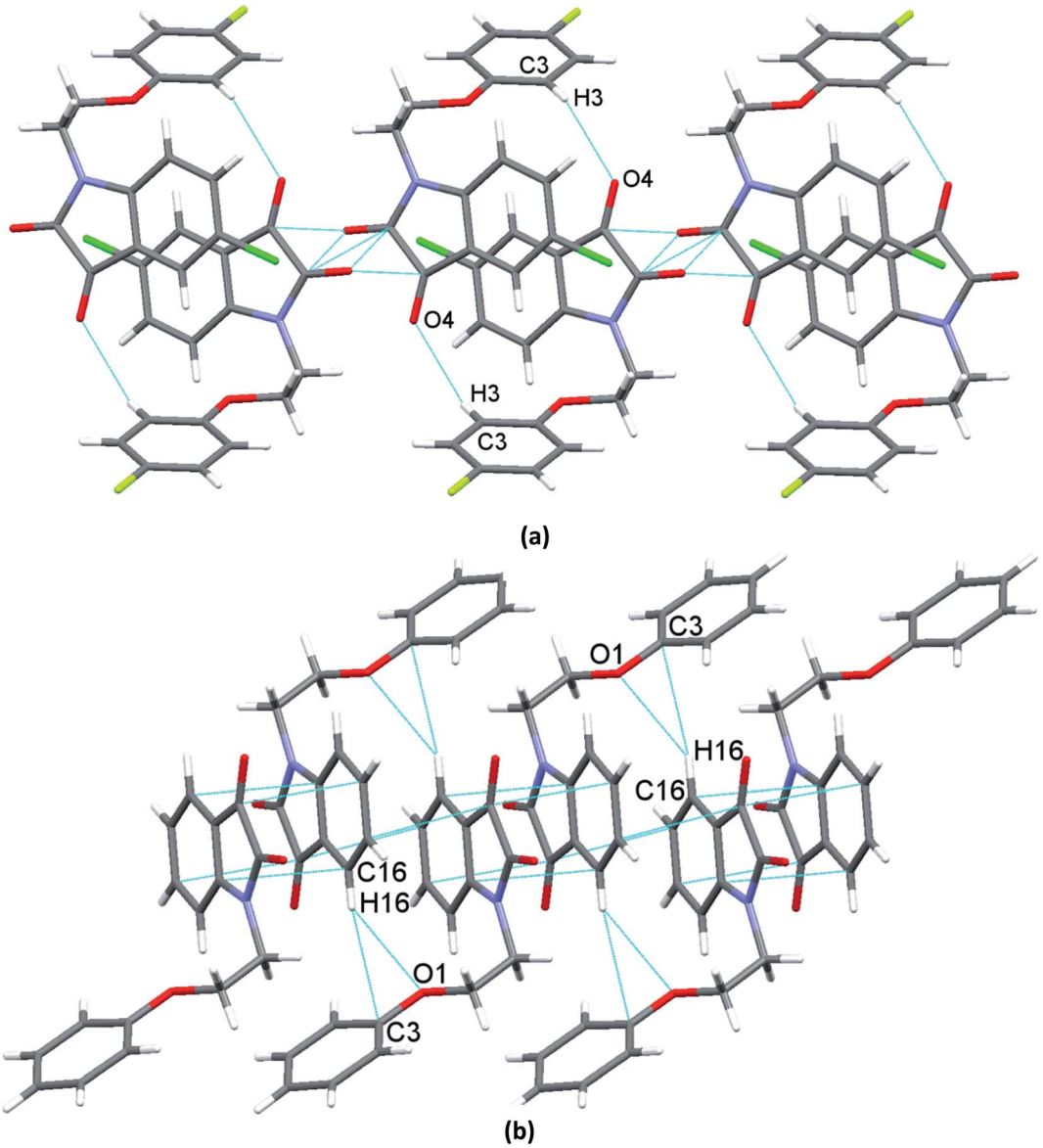

Fig. 4 Showing a) supramolecular 1D-stair like chains of **4** driven by CO···CO, and antiparallel displaced π···π stacking interactions supported by CH···O contacts; b) supramolecular 1D-columnar stacks of **9** driven by antiparallel π···π stacking, and a bifurcated CH···O and CH···π supported antiparallel displaced π···π stacking interactions.

observed distances (*d*) and linearity of involved C–H···O interactions (Table 3), it can be anticipated that these interactions are not structure guided and hence are playing important role in three dimensional solid-state self-assembly of compounds **4** and **9**. However, the existence of CO···CO and antiparallel π···π stacking interactions even in the presence of linear and strong hydrogen bonds indicate their robust nature, consequently offering a unique opportunity to use the compounds **4** and **9** as models to understand the nature of these interactions.

2.2 *In vitro* α-glucosidase inhibition activity of phenoxy pendant isatin 1–12

To reveal the anti-diabetic capability of phenoxy pendant isatins **1–12**, all the twelve compounds were subjected to *in vitro* α-glucosidase inhibition assay. Fortunately, all tested compounds displayed potent anti-diabetic potential (IC_{50} ranging from 5.32–150.13 μM) when compared to the α-glucosidase inhibitor (marketed drug), acarbose ($IC_{50} = 873.34 \pm 1.67$ μM) (Table 4). To establish their structure–activity relationship (SAR) according to variations in the R^1 and R^2 substitutions, these phenoxy pendant isatins can be divided into three group, namely **A**, **B** and **C**. Each group contains four members having same R^2 substituents but different R^1 substituents. Therefore, the difference in α-glucosidase inhibition activity among a group can be dedicated to the nature of R^1 substituents.

Group **A** members, compounds **1–4** (R^2 = Cl) with different R^1 substituents showed nearly comparable anti-α-glucosidase potential to the group **B** compounds **5–8** (R^2 = Br). For

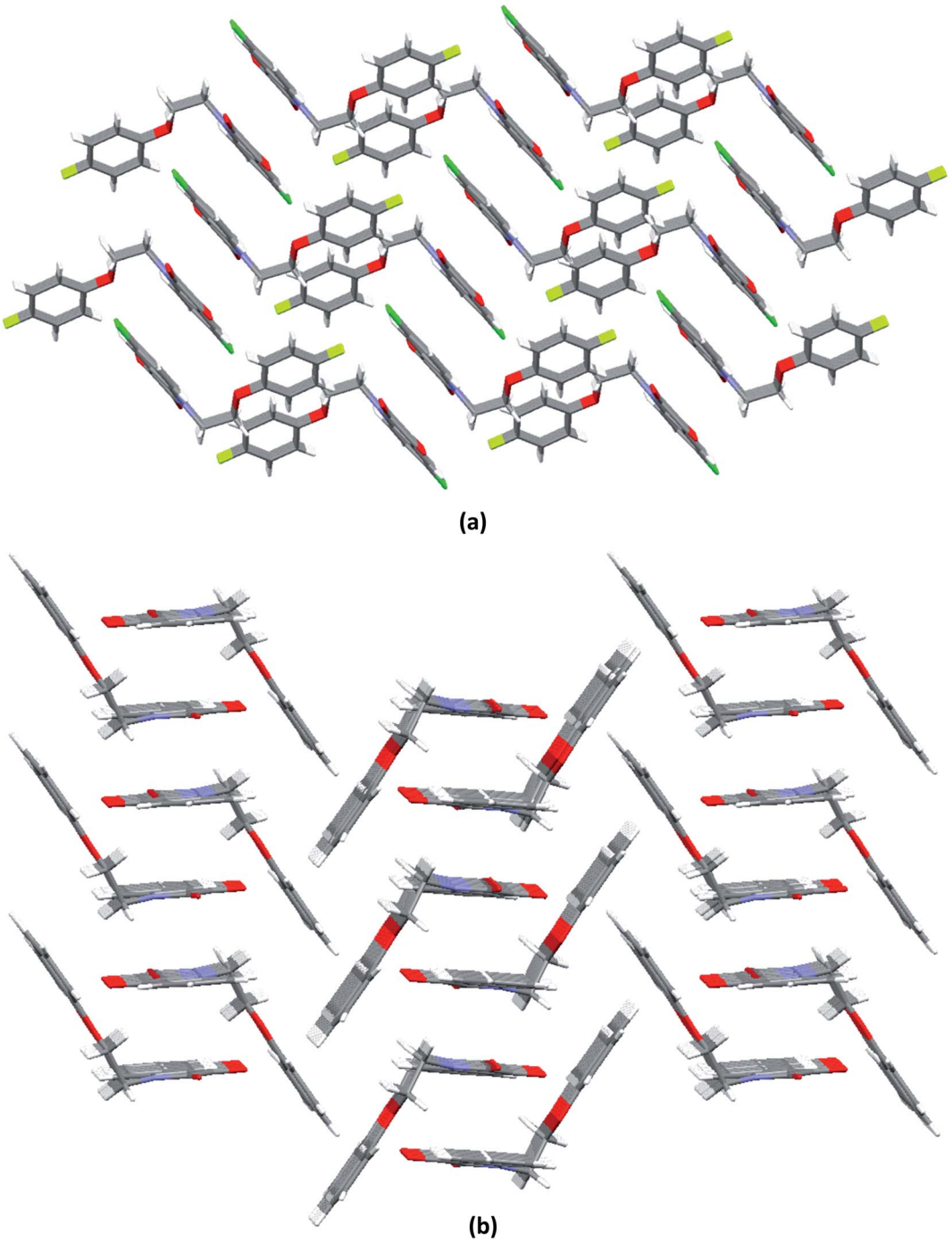

Fig. 5 Molecular packing of phenoxy pendant isatins showing an overall 3D-network structure of, a) **4** (along *a*-axis); b) **9** (along *a*-axis).

example, compound **1** (R^1 = H, R^2 = Cl) exhibited overwhelming inhibition against α-glucosidase ($IC_{50} = 7.87 \pm 0.14$ μM), making it the second most potent anti-α-glucosidase agent in the series. In contrast, the second member of this group *i.e.* compound **2** (R^1, R^2 = Cl) displayed decline in the inhibitory capability against α-glucosidase (IC_{50} = 61.82 ± 0.51 μM). This compound is the second least active anti-diabetic agent among the series. However, the replacement of chloro-substituent with bromo in compound **3** (R^1 = Br, R^2 = Cl) resulted in enhanced the α-glucosidase inhibition (IC_{50} = 21.89 ± 0.16 μM). Interestingly, a minor decrease (IC_{50} = 25.69 ± 0.36 μM *vs.* 21.89 ± 0.16 μM) in activity was observed when fluoro-substituent was introduced in place of bromo-substituent in compound **4** (R^1 = F, R^2 = Cl). The results of this group in general indicate that the presence of more electronegative halogen substituents on the phenyl ring slightly decrease the anti-α-glucosidase potential.

Table 4 α-Glucosidase inhibition of phenoxy pendant isatins [a]

Compounds	R^1	R^2	Percent inhibition (0.5 mM)	$IC_{50} \pm \mu M$ (SEM)
1	H	Cl	92.40	7.87 ± 0.14
2	Cl	Cl	78.19	61.82 ± 0.51
3	Br	Cl	91.87	21.89 ± 0.16
4	F	Cl	91.62	25.69 ± 0.36
5	H	Br	87.59	41.55 ± 0.32
6	Cl	Br	93.64	5.32 ± 0.17
7	Br	Br	93.26	16.17 ± 0.19
8	F	Br	91.74	22.23 ± 0.18
9	H	H	85.00	39.64 ± 0.27
10	Cl	H	91.24	20.28 ± 0.41
11	Br	H	88.76	30.35 ± 0.34
12	F	H	74.81	150.13 ± 0.62
Standard	Acarbose		59.37 (1 mM)	873.34 ± 1.67

[a] N/A = Non active. SEM = Standard error of mean.

Group **B** members, compounds **5–8** (R^2 = Br) displayed an overall slightly better activity when compared to group **A**. The compound **5** (R^1 = H, R^2 = Br) of this group although exhibited potent α-glucosidase inhibition (IC_{50} value 41.55 ± 0.32 μM) but it is ranked the 3rd least potent anti-diabetic candidate among the tested compounds. In this group, compound **6** (R^1 = Cl, R^2 = Br) was found to be the best α-glucosidase inhibitor with exceptional IC_{50} values of 5.32 ± 0.17 μM. In fact, this is the most active compound of the series. Compound **7** (R^1, R^2 = Br) demonstrated slight decrease in the inhibitory potential against α-glucosidase (IC_{50} = 16.17 ± 0.19 μM) as compared to **6**. Similarly, more decrease (IC_{50} = 22.23 ± 0.18 μM was observed for compound **8** (R^1 = F, R^2 = Br) when bromo-substituent on phenyl in **7** was replaced with fluoro-substituent.

Group **C** members, compounds **9–12** (R^2 = H) were found to be the least active when compared with members of other groups. Compound **9** (R^1 = H, R^2 = H) is the 4th least potent anti-α-glucosidase inhibitor of the series (IC_{50} = 39.64 ± 0.27 μM. Importantly, the replacement of R^1 = H with R^2 = Cl has beneficial effect on activity as indicated by the IC_{50} values of compound 10 (IC_{50} = 20.28 ± 0.41 μM). However, a slight decrease in the anti-α-glucosidase inhibition was monitored for compound **11** (IC_{50} = 30.35 ± 0.34 μM), when chloro-substituent was replaced with bromo-substituent. Compound **12** was found to be the least active compound of the group as well as the series. Unlikely, the drastic decline in the anti-diabetic capability was observed for compound **12** (IC_{50} = 150.13 ± 0.62 μM) when bromo-substituent was replaced with fluoro-substituent.

Careful analysis of the IC_{50} values gathered in Table 4 indicate that the introduction of chloro- and bromo-substituents at 5-position of isatin has beneficial influence on α-glucosidase inhibition. However, it is hard to assign the effect of different substituents present at 4-position of phenyloxy pendant on α-glucosidase inhibition. The smaller variations observed in IC_{50} values with different substituents may be attributed to the overall affinity of the compounds to the enzyme binding pockets.

3. Conclusions

In summary, we have evaluated twelve phenoxy pendant isatins **1–12** for their α-glucosidase inhibitory potential as well as the solid-state structures of **4** and **9**. An interesting and unique 1D-supramolecular stair-like chains based on carbonyl···carbonyl and antiparallel displaced π···π stacking interactions, and 1D-columnar stacks based on antiparallel π···π stacking interactions are observed in the solid state self-assembly of compounds **4** and **9**, respectively. Most importantly, the solid-state structure of **4** represent the only example where both one-sided CO···CO and very recently discovered reciprocal CO···CO interactions are observed together. The existence of CO···CO and antiparallel π···π stacking interactions even in the presence of relatively linear and strong C–H···O interactions indicate their robust nature. Therefore, the structures of **4** and **9** along with our recently reported related structure[63] may serve as models to completely understand the nature of CO···CO and much debated π···π stacking interactions. Comparison of solid state structures reported here and in a previous study[63] indicate that the presence of chloro substitution at position-5 of isatin results in CO···CO and slightly displaced antiparallel π···π stacking rather than mere antiparallel π···π stacking interactions. Efforts in this direction may also lead towards the applications of these interactions (through isatin nucleus) in crystal engineering, materials science, and supramolecular chemistry. Moreover, the *in vitro* biological studies of phenoxy pendant isatins **1–12** showed their high potential of α-glucosidase inhibition potential as indicated by their IC_{50} values ranging from 5.32 ± 0.17 to 150.13 ± 0.62 μM compared to the standard drug, acarbose (IC_{50} = 873.34 ± 1.67). The structure–activity relationship (SAR) studies indicate that the presence of halogen substituents at position-5 of isatin has beneficial effect on biological activity. These compounds with potent α-glucosidase inhibitory activity may prove to be an attractive alternative to control postprandial hyperglycemia.

4. Experimental

4.1 General procedure for the synthesis of phenoxy pendant isatins 1–12[63]

To a stirred solution of isatin/5-substituted isatin (5 mmol) in 10 mL DMF containing two equivalents of anhydrous potassium carbonate was slowly added respective 1-(2-bromoethoxy)-4-substituted benzenes (5.5 mmol) at room temperature and the stirring was continued further for another 6 hours at 60 °C. Thin layer chromatography (TLC) was used to monitor the progress of the reaction. After completion of reaction as indicated by TLC, the reaction mixture was poured into the ice-cold distilled water (25 mL). The precipitates thus appeared were filtered, washed with small amount of water, filtered and dried to get the crude product. The crude product was finally recrystallized from ethanol solvent to yield the pure phenoxy pendant isatins **1–12** in good to excellent yields. Full characterization details of these phenoxy pendant isatins are provided in ref. 63. (Note: compounds in this study and in ref. 63 are same but renumbered as **1** = **PI5**, **2** = **PI6**, **3** = **PI7**, **4** = **PI8**, **5** = **PI9**, **6** = **PI10**, **7** = **PI11**, **8** = **PI12**, **9** = **PI1**, **10** = **PI2**, **11** = **PI3**, **12** = **PI4**).

4.2 Single crystal X-ray analysis

Single crystals of **4** and **9** were mounted on a MiTeGen loop with grease and examined on a Bruker D8 VENTURE APEX diffractometer equipped with a photon 100 CCD area detector at 296 (2) K using graphite-monochromated Mo-K_α radiation ($\lambda = 0.71073$ Å). Data were collected using the APEX-II software[67] integrated using SAINT[68] and corrected for absorption using a multi-scan approach (SADABS).[69] Final cell constants were determined from full least squares refinement of all observed reflections. The structure was solved using direct methods using SHELXS-97 and refined with SHELXL-2018 in the SHELXTL package.[70] All non-H atoms were located from the subsequent difference maps and refined anisotropically. H-atoms were added at calculated positions and refined with a riding model. The structures of **4** and **9** been deposited with The Cambridge Crystallographic Data Centre (CCDC deposition numbers are 2175052–2175053). The details of the X-ray crystal data and the structure solution as well as the refinement are given in Table 1.

4.3 *In vitro* α-glucosidase inhibition assay

α-Glucosidase (E.C.3.2.1.20) enzyme (*Saccharomyces cerevisiae*) inhibition assay of phenoxy pendant isatins **1–12** was performed by using 0.1 M phosphate buffer (pH 6.8) at 37 °C.[71] The enzyme (0.2 μ/mL) was incubated in phosphate buffered saline with different concentrations of compounds **1–12** at 37 °C for 15 min. The substrate (0.7 mM, *p*-nitrophenyl-α-D-glucopyranoside) was then added and the variation in absorbance at 400 nm was observed for 30 min using a spectrophotometer (xMark™ Microplate Spectrophotometer, BIO-RAD). The phenoxy pendant isatins **1–12** were substituted with DMSO-d_6 (7.5% final) in the control. Acarbose was used as the reference inhibitor. The % inhibition was calculated by using the following formula:

$$\%\ \text{Inhibition} = 100 - (\text{OD test well/OD control}) \times 100$$

4.4 Statistical analysis

The SoftMax Pro package and Excel were utilized in order to statistically analyze the results.

The % inhibition was calculated by using the following formula.

$$\%\ \text{Inhibition} = 100 - (\text{OD}_{\text{test compound}}/\text{OD}_{\text{Control}}) \times 100$$

Finally, EZ-FIT (Perrella Scientific, Inc., USA) was used for IC_{50} calculations.

Conflicts of interest

There are no conflicts to declare.

Acknowledgements

S. M. and M. M. N. are grateful to Higher Education Commission (HEC) of Pakistan and The World Academy of Sciences (TWAS) for financial support through Project No. 13-419 RG/PHA/AS_CUNESCO FR: 3240279216.

References

1 R. W. Newberry and R. T. Raines, *Acc. Chem. Res.*, 2017, **50**, 1838–1846.
2 T. Steiner, *Angew. Chem., Int. Ed.*, 2002, **41**, 48–76.
3 W. Kabsch and C. Sander, *Biopolymers*, 1983, **22**, 2577–2637.
4 L. Pauling and R. B. Corey, *Proc. Natl. Acad. Sci. U. S. A.*, 1951, **37**, 251–256.
5 L. Pauling, R. B. Corey and H. R. Branson, *Proc. Natl. Acad. Sci. U. S. A.*, 1951, **37**, 205–211.
6 D. J. Pascoe, K. B. Ling and S. L. Cockroft, *J. Am. Chem. Soc.*, 2017, **139**, 15160–15167.
7 B. R. Beno, K. S. Yeung, M. D. Bartberger, L. D. Pennington and N. A. Meanwell, *J. Med. Chem.*, 2015, **58**, 4383–4438.
8 B. K. Sarma, D. Manna, M. Minoura and G. Mugesh, *J. Am. Chem. Soc.*, 2010, **132**, 5364–5374.
9 B. K. Sarma and G. Mugesh, *Chem.–Eur. J.*, 2008, **14**, 10603–10614.
10 B. K. Sarma and G. Mugesh, *J. Am. Chem. Soc.*, 2007, **129**, 8872–8881.
11 M. Iwaoka, H. Komatsu, T. Katsuda and S. Tomoda, *J. Am. Chem. Soc.*, 2004, **126**, 5309–5317.
12 R. W. Newberry and R. T. Raines, *Acc. Chem. Res.*, 2017, **50**, 1838–1846.
13 S. Blanco and J. C. Lopez, *J. Phys. Chem. Lett.*, 2018, **9**, 4632–4637.
14 H. B. Burgi, J. D. Dunitz and E. J. Shefter, *J. Am. Chem. Soc.*, 1973, **95**, 5065–5067.
15 H. B. Burgi, J. D. Dunitz and E. Shefter, *Acta Crystallogr., Sect. B: Struct. Crystallogr. Cryst. Chem.*, 1974, **30**, 1517–1527.
16 H. B. Burgi, J. D. Dunitz and J. M. Lehn, *Tetrahedron*, 1974, **30**, 1563–1572.
17 F. H. Allen, C. A. Baalham, J. P. M. Lommerse and P. R. Raithby, *Acta Crystallogr., Sect. B: Struct. Sci.*, 1998, **54**, 320–329.
18 L. E. Bretscher, C. L. Jenkins, K. M. Taylor, M. L. DeRider and R. T. Raines, *J. Am. Chem. Soc.*, 2001, **123**, 777–778.
19 C. Fufezan, *Proteins: Struct., Funct., Genet.*, 2010, **78**, 2831–2838.
20 S. K. Singh and A. Das, *Phys. Chem. Chem. Phys.*, 2015, **17**, 9596–9612.
21 P. H. Maccallum, R. Poet and E. J. Milner-White, *J. Mol. Biol.*, 1995, **248**, 361–373.
22 P. H. Maccallum, R. Poet and E. J. Milner-White, *J. Mol. Biol.*, 1995, **248**, 374–384.
23 B. Sahariah and B. K. Sarma, *Chem. Sci.*, 2019, **10**, 909–917.
24 (*a*) A. Rahim, P. Saha, K. K. Jha, N. Sukumar and B. K. Sarma, *Nat. Commun.*, 2017, **8**, 78; (*b*) A. Rahim, B. Sahariah and B. K. Sarma, *Org. Lett.*, 2018, **20**, 5743–5746.
25 C. R. Martinez and B. L. Iverson, *Chem. Sci.*, 2012, **3**, 2191–2201.
26 S. Grimme, *Angew. Chem., Int. Ed.*, 2008, **47**, 3430–3434.
27 J. W. Bloom and S. E. Wheeler, *Angew. Chem., Int. Ed.*, 2011, **50**, 7847–7849.

28 H. Li, X. Zhang and W. Zu, *J. Appl. Phys.*, 2014, **115**, 054510.
29 M. Mas-Torrent and C. Rovira, *Chem. Rev.*, 2011, **111**, 4833–4856.
30 R. A. Bissell, E. Córdova, A. E. Kaifer and J. F. Stoddart, *Nature*, 1994, **369**, 133–137.
31 D. Yan, A. Delori, G. O. Lloyd, T. Friščić, G. M. Day, W. Jones, J. Lu, M. Wei, D. G. Evans and X. Duan, *Angew. Chem., Int. Ed.*, 2011, **50**, 12483–12486.
32 S. Burley and G. Petsko, *Adv. Protein Chem.*, 1988, **39**, 125–189.
33 R. Bhattacharyya, U. Samanta and P. Chakrabarti, *Protein Eng.*, 2002, **15**, 91–100.
34 L. M. Salonen, M. Ellermann and F. Diederich, *Angew. Chem., Int. Ed.*, 2011, **50**, 4808–4842.
35 S. Burley and G. A. Petsko, *Science*, 1985, **229**, 23–28.
36 W. Saenger, in *Principles of Nucleic Acid Structure*, Springer, 1984, pp. 1–8.
37 R. Kakkar, *MedChemComm*, 2019, **10**, 351–368.
38 R. Nath, S. Pathania, G. Grover and M. J. Akhtar, *J. Mol. Struct.*, 2020, 128900.
39 G. S. Singh and Z. Y. Desta, *Chem. Rev.*, 2012, **112**, 6104–6155.
40 M. N. Ahmed, M. Arif, F. Jabeen, H. A. Khan, K. A. Yasin, M. N. Tahir, A. Franconetti and A. Frontera, *New J. Chem.*, 2019, **43**, 8122–8131.
41 A. T. Kharroubi and H. M. Darwish, *World J. Diabetes*, 2015, **6**, 850–867.
42 P. T. O'gara, F. G. Kushner, D. D. Ascheim, D. E. Casey Jr, M. K. Chung, J. A. De Lemos, S. M. Ettinger, J. C. Fang, F. M. Fesmire and B. A. Franklin, *Circulation*, 2013, **127**, 529–555.
43 X. Zhao, Y. Wang, R. Chen, J. Li, J. Zhou, C. Liu, P. Zhou, Z. Sheng, Y. Chen and L. Song, *Cardiovasc. Diabetol.*, 2021, **20**, 1–18.
44 C. Mora-Fernández, V. Domínguez-Pimentel, M. M. de Fuentes, J. L. Górriz, A. Martínez-Castelao and J. F. Navarro-González, *J. Physiol.*, 2014, **592**, 3997–4012.
45 E. Mensah and E. Kohner, *Topic. Endocrinol.*, 2002, **19**, 14–18.
46 W. H. Gispen and G.-J. Biessels, *Trends Neurosci.*, 2000, **23**, 542–549.
47 N. Vazzana, P. Ranalli, C. Cuccurullo and G. Davì, *Thromb. Res.*, 2012, **129**, 371–377.
48 Y. Kong, F. Wang, J. Wang, C. Liu, Y. Zhou, Z. Xu, C. Zhang, B. Sun and Y. Guan, *Front. Aging Neurosci.*, 2020, **12**, 217.
49 A. Hussain and A. J. M. Boulton, *Diabetes Res. Clin. Pract.*, 2020, **167**, 108339.
50 C. Proença, M. Freitas, D. Ribeiro, S. M. Tomé, E. F. Oliveira, M. F. Viegas, A. N. Araújo, M. J. Ramos, A. M. Silva and P. A. Fernandes, *J. Enzyme Inhib. Med. Chem.*, 2019, **34**, 577–588.
51 S. R. Joshi, E. Standl, N. Tong, P. Shah, S. Kalra and R. Rathod, *Expet Opin. Pharmacother.*, 2015, **16**, 1959–1981.
52 R. Tundis, M. R. Loizzo and F. Menichini, *Mini Rev. Med. Chem.*, 2010, **10**, 315–331.
53 L. Gong, D. Feng, T. Wang, Y. Ren, Y. Liu and J. Wang, *Food Sci. Nutr.*, 2020, **8**, 6320–6337.
54 I. Abbasi, H. Nadeem, A. Saeed, H. A. A. Kharl, M. N. Tahir and M. M. Naseer, *Bioorg. Chem.*, 2021, **110**, 105385.
55 S. Khatoon, A. Aroosh, A. Islam, S. Kalsoom, F. Ahmad, S. Hameed, S. W. Abbasi, M. Yasinzai and M. M. Naseer, *Bioorg. Chem.*, 2021, **110**, 104816.
56 H. Pervez, N. Khan, J. Iqbal, S. Zaib, M. Yaqub, M. N. Tahir and M. M. Naseer, *Heterocycl. Commun.*, 2018, **24**, 51–58.
57 M. Zia, S. Hameed, A. Frontera, E. Irran and M. M. Naseer, *CrystEngComm*, 2021, **23**, 3144–3151.
58 M. M. Naseer, M. Hussain, A. Bauzá, K. M. Lo and A. Frontera, *ChemPlusChem*, 2018, **83**, 881–885.
59 M. M. Naseer, A. Bauzá, H. Alnasr, K. Jurkschat and A. Frontera, *CrystEngComm*, 2018, **20**, 3251–3257.
60 M. Hussain, A. Bauzá, A. Frontera, K. M. Lo and M. M. Naseer, *CrystEngComm*, 2018, **20**, 150–154.
61 H. Pervez, M. Ahmad, T. B. Hadda, L. Toupet and M. M. Naseer, *J. Mol. Struct.*, 2015, **1098**, 124–129.
62 R. Jawaria, M. Hussain, Z. Shafiq, H. B. Ahmad, M. N. Tahir, H. A. Shad and M. M. Naseer, *CrystEngComm*, 2015, **17**, 2553–2561.
63 S. Mehreen, A. Ullah, H. Nadeem, N. Deged and M. M. Naseer, *RSC Adv.*, 2022, **12**, 1788–1796.
64 A. Bondi, *J. Phys. Chem.*, 1964, **68**, 441–451.
65 G. R. Desiraju, *Acc. Chem. Res.*, 1996, **29**, 441–449.
66 R. Custelcean, N. L. Engle and P. V. Bonnesen, *CrystEngComm*, 2007, **9**, 452–455.
67 APEX suite of crystallographic software. *APEX 2 Version.4*. Bruker AXS Inc., Madison,. Wisconsin, USA, 2008.
68 Bruker SAINT, *version V8.34A*, Bruker AXS Inc., Madison, Wisconsin, USA, 2013.
69 G. M. Sheldrick, *SADABS. Version 2.03*. University of Göttingen, Germany, 2002.
70 (*a*) G. M. Sheldrick, *Acta Crystallogr.*, 1990, **A46**, 467; (*b*) G. M. Sheldrick, *Acta Crystallogr.C*, 2015, **27**, 3.
71 M. I. Choudhary, S. Shah, S. N. Khan and M. T. H. Khan, *Steroids*, 2010, **75**, 956–966.